BIOMASS ESTIMATION ALONG A CLIMATIC GRADIENT USING MULTI-FREQUENCY POLARIMETRIC RADAR VEGETATION INDEX

Geba Jisung Chang[1*], Yisok Oh[2], and Maxim Shoshany[1]

1 Faculty of Civil and Environmental Engineering Department, Technion, Israel Institute of Technology, Haifa, 32000, Israel

2 School of Electronic and Electrical Engineering, Hongik University, South Korea

*Corresponding author: wavegeba@gmail.com

Commission III, WG III/10

KEY WORDS: ALOS-PALSAR, Biomass, multi-frequency polarimetric radar vegetation index, Sentinel-1, shrublands

ABSTRACT:

Monitoring biomass changes in the Mediterranean ecosystems is important for better understanding their responses to climatic and anthropogenic changes. Multi-frequency SAR data (L-band PASLAR and C-band Sentinel-1) is investigated for developing a biomass estimation model along a climatic gradient in Israel. First, the relationships between biomass and transmissivity at various frequencies are discussed. Multi-frequency polarimetric radar vegetation index (MPRVI) is then proposed utilizing the ensemble average of degree of polarization and cross-polarized backscattering coefficients. After randomly partitioning the data for training set and testing set, the new MPRVI-based biomass model is evaluated. It shows a good agreement with reference biomass data with an r-square of 0.899 and a root-mean-squared error (RMSE) of 0.381 kg/m^2 and with a relative RMSE (RRMSE) of 10.8%.

1. INTRODUCTION

Mediterranean ecosystems along climatic gradients are characterized by high diversity of plant such as woodlands, dense shrublands, open shrublands, dwarf shrublands, and arid vegetation (Safriel, 2009; Shoshany, 2000). Mapping biomass for extensive regions along the Mediterranean-to-arid climatic gradient is instrumental for studying desertification and biodiversity changes and may play an essential role in understanding water availability, ecosystem changes, and their response to the global carbon cycle and climate change (Chang and Shoshany, 2017; Santi et al., 2017; Shoshany and Karnibad, 2015).

Remote sensing is a primary information source for assessing such responses at wide regional extents (Shoshany, 2000). However, the extraction of biophysical information, including biomass, from remotely sensed data, is complex in Mediterranean areas due to their high geodiversity (high fragmentation and heterogeneity) (Santi et al., 2017; Sternberg and Shoshany, 2001). Optical sensor data have been widely used at different spatial resolutions; however, it provides information mainly for the upper vegetation layer because of its shallow penetration into the moderate-to-highly dense vegetation canopies (Guyot et al., 1989; Lu, 2006; Prabhakara et al., 2015; Shoshany and Karnibad, 2015; Chang et al., 2022). Since microwaves signal penetrate deeper into canopy layer than optical radiation, synthetic aperture radars (SAR) have been used for remote sensing of biomass, and it was proven that radar parameters such as backscattering coefficient and polarimetric coherence offer relatively high correlation with biomass (Le Toan et al., 1992; Neumann et al., 2012; Sarker et al., 2013). While radar backscatter models are well developed with input parameters including forest and shrubland biomass, the assessment of above-ground biomass (AGB) over a wide region in the Mediterranean is most challenging due to the high spatiotemporal variability of shrubs and background effects such as topography and surface roughness (Eisfelder et al., 2012; Lu, 2006a; Shoshany et al., 2000).

Polarimetric radar vegetation index (PRVI) was proposed by Chang et al. (2018) utilizing the degree of polarization (DOP) and the cross-polarized backscattering coefficients:

$$PRVI = (1 - DOP) \cdot \sigma_{hv}^{o} \tag{1}$$

where DOP is the average of DOPH (degree of polarization for hh- polarization) and DOPV (degree of polarization vv-polarization) for full (or quad) polarization SAR data, and σ_{hv}^{o} is the cross-polarized backscattering coefficient.

PRVI shows a good performance for estimating biomass, by reducing the background effect and moderating the direct scattering effect (Chang et al., 2018). In addition, many studies have indicated that combining multi-frequencies (different wavelengths) shows a better performance than a single frequency for mapping wide range of biomass levels (Ferrazzoli et al., 1997; Jiao et al., 2010; Naidoo et al., 2015; Saatchi et al., 2007; Santi et al., 2017).

Accordingly, this study aims to develop a biomass estimation model based on PRVI by using multi-frequency SAR data for wide regional mapping along a climatic gradient in the South-Eastern Mediterranean region. Taking into account the varying transmissivity characteristics of different frequencies, a technique for improving accuracy by combining multi-frequency SAR data has been studied. Our research is focused on dual-polarization data due to wide availability and low cost of this data.

2. STUDY AREA AND REMOTE SENSING DATA

2.1 Study area (Israel)

The South-Eastern Mediterranean region (Israel) represents a typical Mediterranean-to-arid transition zone from a sub-humid Mediterranean climate to a desert, where the mean annual rainfall ranges from above 600 mm to below 100 mm (Figure 1) (Shoshany et al., 1996; Sternberg and Shoshany, 2001). Vegetation patterns consist of four life forms in this area:

---

* Corresponding author

woodlands (mainly *Pinus halepensis*), taller than 5 m with average biomass of 8 kg/m^2; shrubs (dominant species are *Pistacia lentiscus* and *Rhamnus palaestinus*), with a hight range of 0.5 m - 5 m and average biomass of 4.5 kg/m^2; dwarf shrubs (such as *Sarcopoterium spinosum* and *Thymelaea hirsuta*), with heights less than 0.5 m and an average biomass of 0.7 kg/m^2; herbaceous plants, with maximum biomass of 0.8 kg/m^2 (Svoray et al., 2001). These vegetation types vary due to precipitation and magnitude and frequency of human disturbances. According to the precipitation variation across the gradient zones and the intensity of human disturbance, the shrubland biomass varies approximately from 0.5 kg/m^2 to 5.0 kg/m^2.
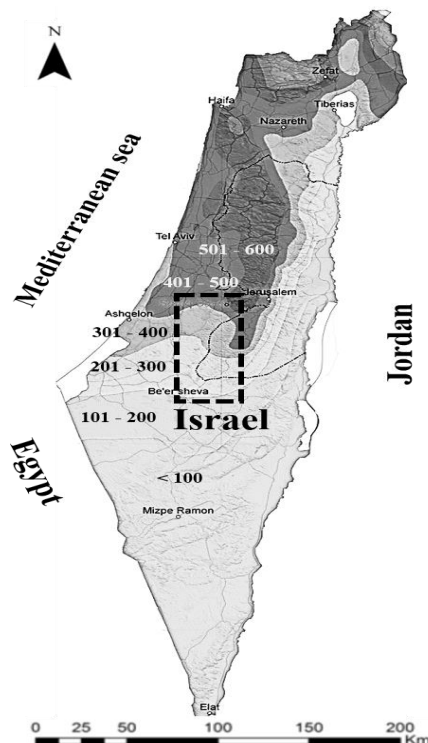
Figure 1. The study area with field experiments sites is marked with a rectangular box. The contour indicates mean annual precipitations (mm/year).

2.2 Remote sensing data

Table I shows the remote sensing data used in this study: dual-polarization L-band ALOS-PALSAR2, dual-polarization C-band Sentinel-1, and mean annual precipitation (MAP). The SRTM (1 arc-second) elevation data was applied to SAR data for terrain correction for PALSAR2 and Sentinel-1. Landsat 8 data were acquired for land classification. All the remote sensing data were co-registered in 10-meter spatial resolution (WGS84/UTM) by ENVI 5.5

Data	Descriptions	Year
ALOS PALSAR2	L-band, dual-pol (HH, HV) (25 m)	2017 (July)
Sentinel-1 GRD	C-band, dual-pol (VV, VH) (10 m)	2017 (July, Sep.)
Landsat 8	Multispectral data (30 m)	2017 (July)
SRTM	Elevation (1 arc-second)	-
Precipitation	17 years	1994~2010

Table 1. Remote sensing data.

2.3 Reference biomass

Numerous allometric models have been suggested to provide an adequate methodological solution for biomass estimation of shrubs and trees based on their geometric properties (Chave et al., 2014; Conti et al., 2019; He et al., 2018; Le Toan et al., 2011; Pereira et al., 1995; Sternberg and Shoshany, 2001).
The average shrub biomass allocation of all species combined was 9.1~27.6% of leaf biomass and 72.4~90.9% of the woody biomass (Sternberg and Shoshany, 2001). Shrub stems (or trunks) and branches are therefore the dominant component of shrub' volume. Here we used the allometric model presented by Pereira (Pereira et al., 1995):

$$B (\text{shrub}) = 0.642 \times h^{0.0075} \times d^{2.49} \qquad (2)$$

where h is the shrub's height and d is its diameter.

Forty-seven ROIs (regions of interest) of shrublands in the study area, 100m by 100m of each ROI, were selected representing local areas of low disturbance. Their biomass was calculated by combining high-resolution orthophoto images and field measurements (Chang and Shoshany, 2017).
The average of tall tree biomass allocations of most species was determined mainly by 72.6% of trunks, followed by 23.8% of branches and 3.4% of foliage (Vargas-Larreta et al., 2017). For estimating tree biomass in this paper, we utilized the following model of He et al. (2018) using the trunk diameter as an independent variable:

$$B (\text{tree}) = 0.0097 DBH^{2.113} + 0.0073 DBH^{2.876} + 0.0913 DBH^{2.386} \quad (3)$$

where DBH is a diameter at breast height for a tree.

Ten ROIs with relatively homogeneous tree density in the study area were selected for utilizing this method. For each ROI, five (or six) trees were measured within 50m by 50m between February and April 2019.

3. MULTI-FREQUENCY RADAR VEGETATION INDEX

The microwave transmissivity (horizontal co-polarization) relationships with biomass are shown in Figure 2 (Entekhabi and Moghaddam, 2007; Ulaby et al., 1986). In this study, the C-band and L-band SAR data have been used as primary imagery source data for biomass estimation (Shimada et al., 2009; Torres et al., 2012).
Multivariate linear regression analysis is frequently used by the remote sensing community for bio-physical estimation, using multi-frequency and multi-polarization SAR data (Berninger et al., 2018; Eisfelder et al., 2012; Lu, 2006b). However, it requires the reparameterization of regression coefficients for each site, thus it is very limited for wide areas mapping. The following generalized PRVI presented by Chang et al., (2018) is suggested here as an alternative:

$$B = a_0 + a_1(PRVI) \qquad (4)$$

where a_0 and a_1 are constant coefficients, and B is the biomass in kg/m^2.

While the PRVI was developed based on full-polarimetric data, the dual-polarization based PRVI can be obtained by replacing the DOP (average of DOPH and DOPV) parameters with one of the DOPH and DOPV. The average of DOP and DOPH are alternative to each other with little difference, and the r-square

between the two is 0.952, as obtained from the previous study using the full polarimetric PALSAR data (Chang et al., 2018). Therefore, the PRVI for dual-polarization has the following form, under the assumption of the homogeneously distributed target (Chang et al., 2018; Ulaby et al., 1992, 1986):

$$\text{PRVI}_{\text{dual}} \cong \left\{ 1 - \frac{\left(\sigma^o_{pp} - \sigma^o_{pq} \right)}{\left(\sigma^o_{pp} + \sigma^o_{pq} \right)} \right\} \cdot \sigma^o_{pq} \quad (5)$$

where the subscript pp denotes vv- or hh-polarization, the subscript pq denotes the cross-polarization, and the dual-polairzation combination would be VV+VH or HH+HV.

Consideration of the frequency-dependent transmissivity, a combined PRVI based biomass model using multiple frequency, can be expressed by the extended form of equation (4):

$$B = b_0 + \sum_{k = X,C,L,P} b_k T_k \text{PRVI}_k \quad (6)$$

where T_k indicates the transmissivity at frequency band k, PRVI_k for the polarimetric radar vegetation index, and b_0 and b_k are constant coefficients.

The T_k can be replaced by simple equations derived from the relationships between biomass and transmissivity (Figure 2) at P-, L-, C-, and X-bands (Ulaby et al., 1986):

$$\sum_{k = X,C,L,P} b_k T_k \text{PRVI}_k = (-0.05B + 0.99)\text{PRVI}_P + \left(-0.13B + 0.97 \right)\text{PRVI}_L$$
$$+ (0.99\, e^{-0.65B})\text{PRVI}_C + (1.01\, e^{-1.36B})\text{PRVI}_X \quad (7)$$

Equation (6) and (7) would offer better accuracy with containing the proportion of biomass due to each different penetration depth for each frequency, but they are too complex to be used in developing a biomass model.

The DOP parameter of PRVI is relevant with volume scattering (multiple scattering) than biomass itself (Chang and Shoshany, 2017; Chang et al., 2018). Therefore, equation (6) can be expressed as separating an integral form of DOP and cross-pol backscattering coefficients under the assumption that multiple scattering, according to the wavelengths, is similar. In the multiplication between the transmissivity T and the cross-polarized backscattering coefficient (σ^o_{hv}), the transmissivity T can be ignored since the rate of the change in T with the increase in biomass is much smaller than the changes in 'σ^o_{hv}' with the increase of biomass.

Therefore, equation (7) can be simplified by a new parameter, multi-frequency polarimetric radar vegetation index (MPRVI) which represent multiplying the ensemble average of DOP and cross polarized backscattering coefficient:

$$\text{MPRVI} \cong \left(1 - \langle \text{DOP}_Q \rangle \right) \langle \sigma^o_{VH} \rangle \quad (8)$$

where the subscript Q is H or V for HH+HV or VV+VH dual polarization, respectively, and ⟨ ⟩ denotes the ensemble average for multi-frequency bands.

Utilizing C-band Sentinel-1 and L-band PALSAR2 data, the MPRVI is calculated and assessed with reference to biomass from the previous research (Chang et al., 2018). Figure 3 shows that correlation between the MPRVI (equation 8) and the multiplying PRVI with the characteristic of transmissivity (equation 7) obtains high correlation (r^2: 0.908). Such a high correlation indicates that the proposed MPRVI incorporates the

characteristics of multi-frequencies while taking into account transmissivities. It can replace thus the complicated non-linear equation (7) with the simple form of equation (8) for biomass estimation. Therefore, the biomass model utilizing multi-frequency SAR data can be expressed by the MPRVI, in a modified form of equation (4):

$$B = c_0 + c_1 (\text{MPRVI}) \quad (9)$$

where c_0 and c_1 are constant coefficients.
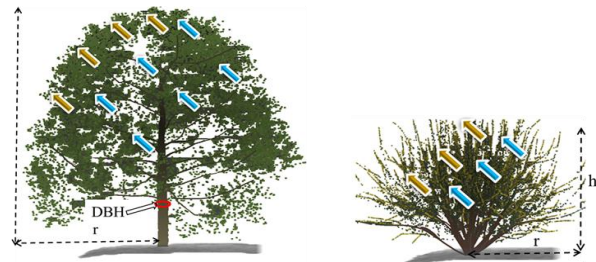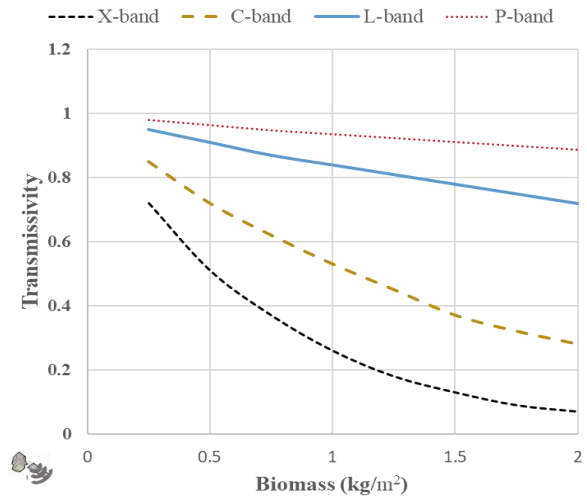
Figure 2. Canopy transmissivity for sample microwave bands (horizontal co-polarization) corresponding to biomass (Ulaby et al., 1986), and structure parameters for woody plants (bottom left for tree and bottom right for shrub).
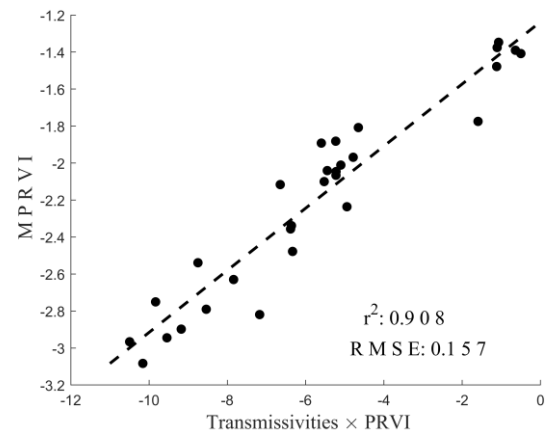
Figure 3. Correlation between the multiplying PRVI with the characteristic of transmissivity (equation 7) and the MPRVI (equation 8).

4. RESULTS AND DISCUSSION

For each ROI, the average of the values extracted for 5 by 5 pixels (50 m by 50 m) was used as radar parameters (backscatters, DOPs, and PRVIs) from the PALSAR and Sentinel-1 data. For a preliminary analysis, the correlations between radar parameters and biomass were analysed by using dual-polarization C-band (DC) Sentinel-1 data, and dual-polarization L-band (DL) PALSAR2 data: $\sigma^o_{VV,DC}$ (r^2: 0.066), $\sigma^o_{VH,DC}$ (r^2: 0.534), DOP_{DC} (r^2: 0.604), $\sigma^o_{HH,DL}$ (r^2: 0.570), $\sigma^o_{HV,DL}$ (r^2: 0.639), and DOP_{DL} (r^2: 0.573). The L-band cross polarized backscattering coefficient ($\sigma^o_{HV,DL}$) and C-band DOP (DOP_{DC}) showed relatively better correlations with biomass than other parameters.

PRVI and MPRVI were calculated and analysed with reference biomass: $PRVI_C$ (r^2: 0.613), $PRVI_L$ (r^2: 0.656), and MPRVI (r^2: 0.739). The PRVI values showed better performance than other radar parameters in both C-band and L-band data. Above all, the MPRVI performed better than single frequency PRVI. These results show that synergetic use of multi-frequency could improve biomass estimation.

4.1 Model fitting

Two unknown coefficients (c_0 and c_1) of equation (9) were obtained by using the regression analysis with allometric biomass data based on the following logarithmic form:

$$\text{Log10 (B)} = 2.58 + 1.37 \text{ MPRVI (dB)} \qquad (10)$$

A simple color composition map was shown in Figure 4 (left) with an RGB image combination (R: MPRVI, G: NDVI, B: HH_L-VV_C), where NDVI was acquired from Landsat data. Green color indicates the vegetated areas and blue shows bare surface regions, and red indicates dense forest regions or urban and rocky regions with high backscattering coefficients.

A MPRVI-based biomass map was generated by equation (10) as shown in Figure 4 (right). The MPRVI was still affected by background effects from rough bare surfaces and rocks, while it was found to be instrumental in reducing the effect of surface roughness compared with other radar parameters. The biomass extracted from the MPRVI based model ranges from 1.1 to 1.8 kg/m² for shrublands where the annual rainfall is above 400 mm/year, and from 0.4 to 1.4 kg/m² for shrubs in the semi-arid region with 200-400 mm/year. The average biomass for forest regions (mostly *Pinus halepensis*) exceeds 3.0 kg/m².

Southern Israel (Negev desert, reddish color in RGB image) is located mostly in the arid region having very low biomass; however, the biomass obtained in practice shows moderate biomass because the MPRVI was overestimated by high cross-polarized backscattering coefficients for very rough surfaces and rocks in the region. For these reasons, the biomass model was not applied in southern Israel (Negev desert) with NDVI values lower than 0.2.

4.2 Model validation

For validation, data set was partitioned randomly into two subsets of 50% for training and testing, using regression leaner toolbox of MATLAB. Figure 5 shows the response plot of the MPRVI based biomass model in log scale. The average of square error was 0.031 for 57 data points. In general, the error level was significant at the relatively low biomass region (semi-arid to arid region). One of the reasons would be the high geodiversity of shrubs (high fragmentation and heterogeneity),
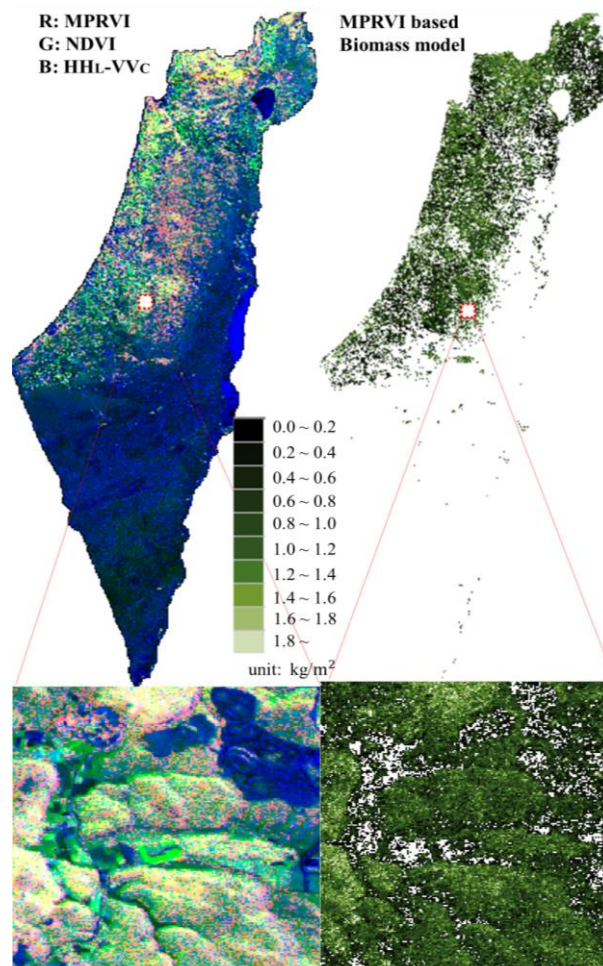
Figure 4. (Left) RGB image (R: MPRVI, Green: NDVI, Blue: $HH_L - VV_C$) with the enlarged area of Ella Valley, and (Right) MPRVI-based biomass maps.

and another reason could be the topography effect (the study area is hilly).

Figure 6 shows the validation of the MPRVI based model with reference to biomass data. Since there were more measurements of shrubs than tall trees, many of the estimated biomass values were less than 2kg/m². Overall, it shows a good agreement with reference biomass including shrubs and tall tree (r-square: 0.899, root-mean-squared error (RMSE): 0.381 kg/m², and relative RMSE (RRMSE): 10.8%).

Most other investigations of remote sensing biomass estimation have tested biomass ranges up to 600 Mg/ha, primarily in forests and dense woodlands, whereas semi-arid shrublands' biomass estimation and mapping is most challenging due to their relatively low biomass, ranging between 0 to 5 kg/m² (50 Mg/ha) (Eisfelder et al., 2012; Vaglio Laurin et al., 2021).

Recently, advanced SAR technology such as PolInSAR, time-series, and integration techniques have been applied to multi-frequencies data to improve biomass estimation (Kraatz et al., 2021; ME and Kumar, 2021; Vaglio Laurin et al., 2021). Future BIOMASS mission (satellite-based P-band SAR data) which is planned to be launched by the European Space Agency in 2022 (Le Toan et al., 2011) would be instrumental for further testing and implementing our methodology.
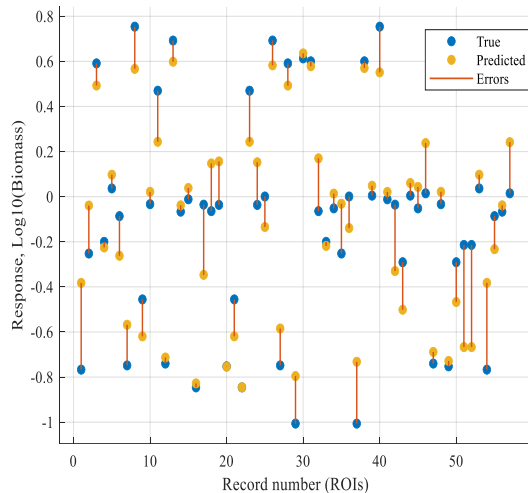
Figure 5. Response plot of the MPRVI based biomass model in log scale.
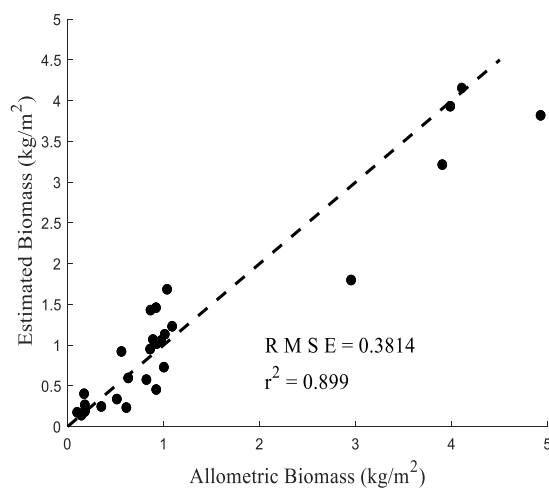
Figure 6. Validation of the MPRVI based biomass model.

5. CONCLUSION

Based on the concept of polarimetric radar vegetation index (PRVI), the multi-frequency polarimetric radar vegetation index (MPRVI) was developed and applied to the semi-arid Mediterranean ecosystem of Israel. Key radar parameters (i.e., the degree of polarization and the cross-polarized backscattering coefficient) for biomass estimation are integrated into the MPRVI as a simple form for biomass estimation by using dual polarization PALSAR2 (L-band) and Sentinel-1 (C-band) data. MPRVI based biomass model shows a high r-square value of 0.899 with reference to biomass.

Our investigation may contribute to improving a wide range of biomass mapping. Further research is needed to apply this model to a wide range of biomass data. Integration techniques by using multi-sources such as optical sensors (multi-spectral), Lidar, Interferometry SAR (InSAR) may improve biomass estimation in a wide range of biomass (e.g. Chang and Shoshany, 2016; Cutler et al., 2012; Vaglio Laurin et al., 2021).

REFERENCES

Berninger, A., Lohberger, S., Stängel, M., Siegert, F., 2018. SAR-based estimation of above-ground biomass and its changes in tropical forests of Kalimantan using L-and C-band. *Remote Sens.* 10, 831.

Chang, G.J., Oh, Y., Goldshleger, N., Shoshany, M., 2022. Biomass estimation of crops and natural shrubs by combining red-edge ratio with normalized difference vegetation index. *J. Applied Remote Sens*. 16, 1–15.

Chang, J., Shoshany, M., 2017. Radar polarization and ecological pattern properties across Mediterranean-to-arid transition zone. *Remote Sens. Environ*. 200.

Chang, J., Shoshany, M., 2016. Mediterranean shrublands biomass estimation using Sentinel-1 and Sentinel-2, in: *International Geoscience and Remote Sensing Symposium* (IGARSS).

Chang, J.G., Shoshany, M., Oh, Y., 2018. Polarimetric Radar Vegetation Index for Biomass Estimation in Desert Fringe Ecosystems. *IEEE Trans. Geosci. Remote Sens.* PP, 1–7.

Chave, J. et. al, 2014. Improved allometric models to estimate the aboveground biomass of tropical trees. *Glob. Chang. Biol.* 20, 3177–3190.

Conti, G., et al., 2019. Developing allometric models to predict the individual aboveground biomass of shrubs worldwide. *Glob. Ecol. Biogeogr*. 28, 961–975.

Cutler, M.E.J., Boyd, D.S., Foody, G.M., Vetrivel, A., 2012. Estimating tropical forest biomass with a combination of SAR image texture and Landsat TM data: An assessment of predictions between regions. *ISPRS J. Photogramm. Remote Sens*. 70, 66–77.

Eisfelder, C., Kuenzer, C., Dech, S., 2012. Derivation of biomass information for semi-arid areas using remote-sensing data. *Int. J. Remote Sens.* 33, 2937–2984.

Entekhabi, D., Moghaddam, M., 2007. Mapping recharge from space: roadmap to meeting the grand challenge. *Hydrogeol. J.* 15, 105–116.

Ferrazzoli, P., Paloscia, S., Pampaloni, P., Schiavon, G., Sigismondi, S., Solimini, D., 1997. The potential of multifrequency polarimetric sar in assessing agricultural and arboreous biomass. IEEE Trans. Geosci. *Remote Sens.* 35, 5–17.

Guyot, G., Guyon, D., Riom, J., 1989. Factors affecting the spectral response of forest canopies: a review. *Geocarto Int.* 4, 3–18.

He, H., Zhang, C., Zhao, X., Fousseni, F., Wang, J., Dai, H., Yang, S., Zuo, Q., 2018. Allometric biomass equations for 12 tree species in coniferous and broadleaved mixed forests, Northeastern China. *PLoS One*. 13, 1–16.

Jiao, X., McNairn, H., Shang, J., Liu, J., 2010. The sensitivity of multi-frequency (X, C and L-band) radar backscatter signatures to bio-physical variables (LAI) over corn and soybean fields, in: *ISPRS TC VII Symposium*—100 Years ISPRS. pp. 317–325.

Kraatz, S., Torbick, N., Jiao, X., Huang, X., Robertson, L.D., Davidson, A., McNairn, H., Cosh, M.H., Siqueira, P., 2021. Comparison between Dense L-Band and C-Band Synthetic Aperture Radar (SAR) Time Series for Crop Area Mapping over a NISAR Calibration-Validation Site. *Agronomy* 11, 273.

Le Toan, T., Beaudoin, A., Riom, J., Guyon, D., 1992. Relating Forest Biomass to SAR Data. *IEEE Trans. Geosci. Remote Sens.* 30, 403–411.

Le Toan, T., Quegan, S., Davidson, M.W.J., Balzter, H., Paillou, P., Papathanassiou, K., Plummer, S., Rocca, F., Saatchi, S., Shugart, H., Ulander, L., 2011. The BIOMASS mission: Mapping global forest biomass to better understand the terrestrial carbon cycle. *Remote Sens. Environ.* 115, 2850–2860.

Lu, D., 2006a. The potential and challenge of remote sensing-based biomass estimation. *Int. J. Remote Sens.* 27, 1297–1328.

ME, B.P., Kumar, S., 2021. PolInSAR decorrelation-based decomposition modelling of spaceborne multifrequency SAR data. *Int. J. Remote Sens.* 42, 1398–1419.

Lu, D., 2006b. The potential and challenge of remote sensing-based biomass estimation. *Int. J. Remote Sens.* 27, 1297–1328.

Naidoo, L., et al., 2015. Savannah woody structure modelling and mapping using multi-frequency (X-, C- and L-band) Synthetic Aperture Radar data. *ISPRS J. Photogramm. Remote Sens.* 105, 234–250.

Neumann, M., Saatchi, S.S., Ulander, L.M.H., Fransson, J.E.S., 2012. Assessing Performance of L- and P-Band Polarimetric Interferometric SAR Data in Estimating Boreal Forest Above-Ground Biomass. *IEEE Trans. Geosci. Remote Sens.* 50, 714–726.

Pereira, J.M.. M.C., Oliveira, T.M.M., Paul, J.C.P.C.P., 1995. Satellite-based estimation of mediterranean shrubland structural parameters. *EARSel Adv. Remote Sens.*

Prabhakara, K., Dean Hively, W., McCarty, G.W., 2015. Evaluating the relationship between biomass, percent groundcover and remote sensing indices across six winter cover crop fields in Maryland, United States. *Int. J. Appl. Earth Obs. Geoinf.* 39, 88–102.

Saatchi, S., Halligan, K., Despain, D.G., Crabtree, R.L., 2007. Estimation of forest fuel load from radar remote sensing. *IEEE Trans. Geosci. Remote Sens.* 45, 1726–1740.

Safriel, U.N., 2009. Status of Desertification in the Mediterranean Region.

Santi, E., Paloscia, S., Pettinato, S., Fontanelli, G., Mura, M., Zolli, C., Maselli, F., Chiesi, M., Bottai, L., Chirici, G., 2017. The potential of multifrequency SAR images for estimating forest biomass in Mediterranean areas. *Remote Sens. Environ.* 200, 63–73.

Sarker, M.L.R., Nichol, J., Iz, H.B., Ahmad, B. Bin, Rahman, A.A., 2013. Forest biomass estimation using texture measurements of high-resolution dual-polarization C-band SAR data. *IEEE Trans. Geosci. Remote Sens.* 51, 3371–3384.

Shimada, M., Isoguchi, O., Tadono, T., Isono, K., 2009. PALSAR radiometric and geometric calibration. *IEEE Trans. Geosci. Remote Sens.* 47, 3915–3932.

Shoshany, M., 2000. Satellite remote sensing of natural Mediterranean vegetation: a review within an ecological context. *Prog. Phys. Geogr.* 24, 153–178.

Shoshany, M., Karnibad, L., 2015. Relative Water Use Efficiency and Shrublands Biomass along a Semi-Arid Climatic Gradient: A Remote Sensing Study. *Remote Sens.* 2283–2301.

Shoshany, M., Karnibad, L., 2014. Remote Sensing of Shrubland Drying in the South-East Mediterranean 1995-2010: Water-Use Efficiency Based Mapping of Biomass Change. *Arid Environ.* 2283–2301.

Shoshany, M., Kutiel, P., Lavee, H., 1996. Monitoring temporal vegetation cover changes in Mediterranean and arid ecosystems using a remote sensing technique: case study of the Judean Mountain and the Judean *Desert. J. Arid Environ.* 33, 9–21.

Shoshany, M., Svoray, T., Curran, P.J., Foody, G.M., Perevolotsky, A., 2000. The relationship between ERS-2 SAR backscatter and soil moisture: generalization from a humid to semi-arid transect. *Int. J. Remote Sens.* 21, 2337–2343.

Sternberg, M., Shoshany, M., 2001. Aboveground biomass allocation and water content relationships in Mediterranean trees and shrubs in two climatological regions in Israel. *Plant Ecol.* 157, 173–181.

Svoray, T., Shoshany, M., Curran, P., Foody, G., Perevolotsky, A., 2001. Relationship between bio-physical parameters of four life-forms and ERS-2 backscatter in the semi-arid zone of Israel. *Int. J. Remote Sens.* 22, 1601–1607.

Torres, R., et al., 2012. GMES Sentinel-1 mission. *Remote Sens. Environ.* 120, 9–24.

Ulaby, F.T., Moore, R.K., Fung, A.K., 1986. Microwave remote sensing: Active and passive. Volume 3-From theory to applications.

Ulaby, F.T., Sarabandi, K., Nashashibi, A., 1992. Statistical properties off the Mueller matrix off distributed targets, in: I*EE Proceedings F* (Radar and Signal Processing). IET, pp. 136–146.

Vaglio Laurin, G., Puletti, N., Tattoni, C., Ferrara, C., Pirotti, F., 2021. Estimated Biomass Loss Caused by the Vaia Windthrow in Northern Italy: Evaluation of Active and Passive Remote Sensing Options. *Remote Sens.* 13, 4924.

Vargas-Larreta, et al., 2017. Allometric equations for estimating biomass and carbon stocks in the temperate forests of North-Western Mexico. Forests 8, 1–20.